On the Impact of Strained PECVD Oxide Layers on Oxide Precipitation in Silicon

G. Kissinger,[1,*,z] D. Kot,[1] M. Lisker,[1] and A. Sattler[2]

[1]*IHP - Leibniz-Institut für innovative Mikroelektronik, 15236 Frankfurt (Oder), Germany*
[2]*Siltronic AG, 81737 Munich, Germany*

PECVD oxide layers with different layer stress ranging from about −305.2 MPa to 39.9 MPa were deposited on silicon wafers with similar concentration of interstitial oxygen. After a thermal treatment consisting of rapid thermal annealing (RTA) and furnace annealing 780°C 3 h + 1000°C 16 h in nitrogen the profiles of the oxide precipitate density were investigated. Supersaturations of self-interstitials as function of layer stress were determined by adjusting modelling results to measured depth profiles of bulk microdefects. The self-interstitial supersaturation generated by RTA at 1250°C and 1175°C at the silicon/oxide interface is increasing linearly with increasing layer stress. Values for self-interstitial supersaturation determined on deposited oxide layers after RTA at 1250°C and 1175°C are very similar to values published for RTO by Sudo et al. An RTA at 1175°C with a PECVD oxide on top of the wafer is a method to effectively suppress oxygen precipitation in silicon wafers. Nucleation anneals carried out at 650°C for 4 h and 8 h did not show any effect of PECVD oxide layers on oxide precipitate nucleation.
© The Author(s) 2019. Published by ECS. This is an open access article distributed under the terms of the Creative Commons Attribution 4.0 License (CC BY, http://creativecommons.org/licenses/by/4.0/), which permits unrestricted reuse of the work in any medium, provided the original work is properly cited. [DOI: 10.1149/2.0141904jss]

Manuscript submitted March 21, 2019; revised manuscript received May 3, 2019. Published May 9, 2019.

It is well known from manufacturing integrated circuits that thermal oxidation of silicon generates supersaturation of self-interstitials for stress release at the growth interface because of the different molecular volume between silicon and silicon oxide. Part of the excess self-interstitials are assumed to segregate to the oxide layer leading to regrowth of the layer, some of them diffuse into the silicon bulk where they can recombine with vacancies or influence precipitation of interstitial oxygen.[1] The self-interstitials diffusing into the silicon bulk can also lead to enhanced diffusion of boron and phosphorus and retarded diffusion of antimony.[2–4] Advanced as well as simplified models describing the retarded and enhanced diffusion of dopants assume that the interstitial supersaturation at the interface silicon/oxide is a function of the oxidation rate.[1,5–8]

In as-grown Czochralski silicon wafers, the interstitial oxygen exists in a supersaturated state. During thermal treatments, it precipitates forming octahedral or plate-like oxide precipitates. Similar to the oxide layers, interstitials are generated during precipitate growth to relieve the strain due to the molecular volume difference between silicon and silicon oxide. The nucleation rate of oxide precipitates is sensitive to supersaturation of intrinsic point defects. While vacancy supersaturation enhances oxygen precipitation self-interstitial supersaturation retards it.[9] Thus, thermal treatment of silicon wafers in oxidizing atmosphere leads to suppression of oxygen precipitation and increased precipitate denuded zones below the silicon surface.[10]

Until now, it is not well understood what the effect of oxide layers, which were just deposited without consumption of silicon, on the generation of intrinsic point defects is. Dunham has analyzed and modeled the interactions of point defects with very thin oxide films under non-oxidizing conditions.[6] However, this is a special case because SiO desorption from the surface is of high impact on the result.

A second issue not well understood is the impact of layer stress on the generation of intrinsic point defects. Stress influences the intrinsic point defects during crystal growth because the equilibrium concentrations of vacancies and self-interstitials depend on stress.[11–13] The diffusivities of vacancies and interstitials in silicon were also found to be dependent on stress.[14,15] However, these effects seem negligible in case of oxide layers with stresses in the MPa range because only stress in the GPa range are of clear impact. Navi and Dunham developed a model which describes the impact of the mechanical behavior of oxide layers on the oxidation kinetics which involves the relaxation of oxides as oxidation proceeds.[16]

In our investigations, we have chosen a deposition method for silicon oxide and not a thermal oxidation in order to investigate the effect of layer stress and separate it from generation of intrinsic point defects during layer growth with silicon consumption. The intrinsic point defects generated were analyzed via their impact on oxygen precipitation. On the one side, oxygen precipitation serves for analysis of the point defect behavior, and on the other side the results are important for controlling oxygen precipitation during device processing.

Experimental

Silicon wafers 200 mm in diameter and 625 μm thick, B-doped with a resistivity of about 10 Ωcm and a concentration of interstitial oxygen in the range 6.3–6.6 × 10^{17} cm^{-3} (conversion factor 2.45 × 10^{17} cm^{-2}) were used for the experiments. On these wafers, silicon oxide layers were deposited by PECVD (plasma enhanced chemical vapor deposition). With this method, the oxide layers are deposited from the gas phase at about 380°C on the front wafer surface only and it is possible to adjust the layer stress independent of the layer thickness. Even, slightly tensile strained oxide layers can be deposited by PECVD. This allowed us to investigate the impact of the layer stress on the oxygen precipitation and on the generation of excess self-interstitials from the interface oxide/silicon. We deposited oxide layers of thicknesses in the range 799–869 nm with layer stresses ranging from −305.2 MPa to 39.9 MPa. The layer stress was measured using a FSM 128 stress and wafer bow/warp measurement system and calculated according to Stoney's equation.[17] In addition to the initial concentration of interstitial oxygen of the silicon substrate wafers, all thicknesses and layer stresses of the PECVD oxide layers used in the experiments can be found in Tables I and II.

Two different kinds of thermal treatments were applied, a rapid thermal anneal (RTA) at both 1250°C or 1175°C for 30s in pure Ar, in order to prevent any further oxidation at the high temperatures, and a nucleation anneal at 650°C for both 4 h and 8 h in nitrogen. After the first step, the RTA or the nucleation anneal, a so-called BMD test consisting of an anneal at 780°C for 3h in N_2 for stabilization of oxide precipitate nuclei and a growth anneal at 1000°C for 16h in N_2 were carried out. For the RTA, full wafers were used and for all other thermal treatments 3 cm x 3 cm pieces were cut from the wafers.

The density of bulk microdefects (BMDs), which are oxide precipitates with or without secondary defects, was determined by preferential etching of (110) cleavage planes perpendicular to the (100) wafer surface using Secco etchant.[18] Depth profiles were generated measuring the BMD density across the cleavage plane.

Fourier transform infrared (FTIR) spectrometry was used to analyze and compare the oxide layers used in the experiments. The spectra were recorded against silicon samples of the same wafer without oxide

*Electrochemical Society Member.
[z]E-mail: gkissinger@ihp-microelectronics.com

Downloaded on 2019-05-10 to IP 194.95.141.200 address. Redistribution subject to ECS terms of use (see ecsdl.org/site/terms_use) unless CC License in place (see abstract).

Table I. Interstitial oxygen concentration of the silicon substrate, layer stress and thickness of the PECVD oxide layers, and Temperature of the RTA soak.

O_i (10^{17} cm^{-3})	Average layer stress (MPa)	Average layer thickness (nm)	RTA temperature (°C)
6.4	−1.4	799	1250
6.6	0.7	811	1175
6.4	−125.5	826	1250
6.5	−127.1	825	1175
6.5	−263.7	850	1250
6.5	−263.5	851	1175
6.5	−305.2	868	1250
6.5	−304.7	869	1175
6.5	no layer	0	1250
6.4	no layer	0	1175

layer using a resolution of 4 cm^{-1} and an aperture of 1 mm. A Bruker Vertex 80v was used for the measurements.

Results

Experimental results.—In the beginning, we compare the FTIR spectra of oxide layers with different layer stress. It can be seen in Fig. 1 that all spectra are very similar. In all spectra, we can find the two absorption bands at 1072 cm^{-1} and 816 cm^{-1} which can be assigned to SiO_2.[19] The band of Si-H typically located in the range 2260–2280 cm^{-1}[19] was not found. The band of SiO-H is present in all samples of as-deposited wafers. As can be seen in Fig. 2 (left), the maximum absorption coefficient decreases with increasing compressive stress and remains constant for high stress. The SiO-H band was deconvoluted into two bands, one at about 3675 cm^{-1} and the other at about 3625 cm^{-1}. Similar bands were observed by Adams et al.[19] The corresponding hydrogen concentration was calculated using the conversion factor of Ref. 19 which is very similar to the conversion factor of Rostaing et al.[20] for SiO-H. As shown in Fig. 2 (right), the hydrogen concentration is increased for the layers with low compressive stress. These were deposited with lower RF plasma power which results in higher concentration of hydrogen in the layer. After nucleation anneal at 650°C for 4 h as well as after RTA at 1175°C for 30 s the SiO-H band was not observed anymore. Obviously, hydrogen evaporated from the layers.

Table II. Interstitial oxygen concentration of the silicon substrate, layer stress and thickness of the PECVD oxide layers.

O_i (10^{17} cm^{-3})	Average layer stress (MPa)	Average layer thickness (nm)
6.4	39.9	816
6.3	−34.3	802
6.4	−161.0	818
6.3	−247.5	833
6.3	no layer	0

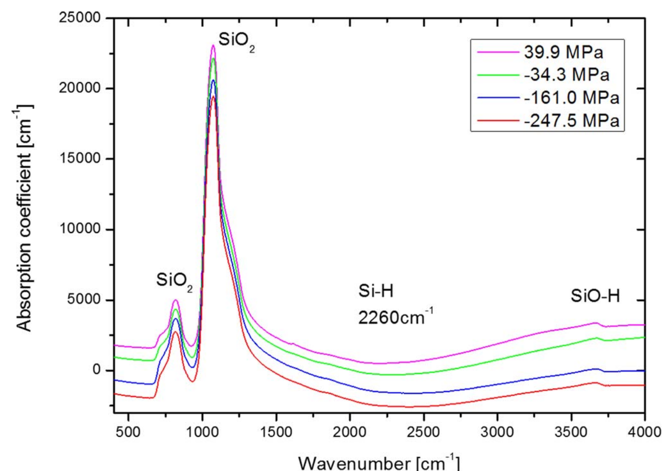

Figure 1. FTIR spectra of as-deposited oxide layers with different average layer stress.

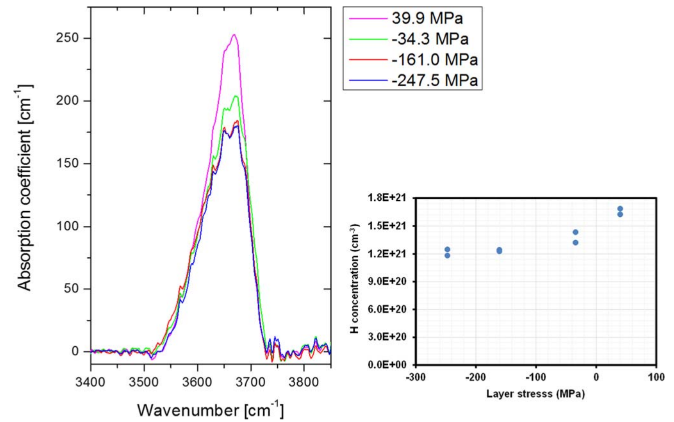

Figure 2. Absorption band of SiO-H shown for different layer stress (left) and corresponding hydrogen concentration of the oxide layers determined according to Ref. 19 (right).

The layers are compressively strained while the substrate is tensile strained on the front side and compressively stressed on the reverse side. The stress system is fully biaxial. Close to the center of the wafer, a so-called neutral zone with zero stress exists. The wafer stress reaches maxima with reverse sign on both surfaces. The maximum substrate stress σ_s can be calculated from the film stress σ_l via the following relation[21]

$$\sigma_s = -\sigma_l \cdot 4 \cdot \frac{d_l}{d_s} \quad [1]$$

with d_l and d_s being the thicknesses of the oxide layer and silicon substrate, respectively. The silicon substrate stress is about three orders of magnitude lower than the compressive oxide layer stress.

The results of the BMD density depth profiles for samples obtained from wafers with oxide layers of different layer stress after RTA at 1250°C and BMD test can be found in Fig. 3. One of the samples was an as-grown wafer without oxide layer. The effect of the differently stressed layers on oxygen precipitation is marked. With

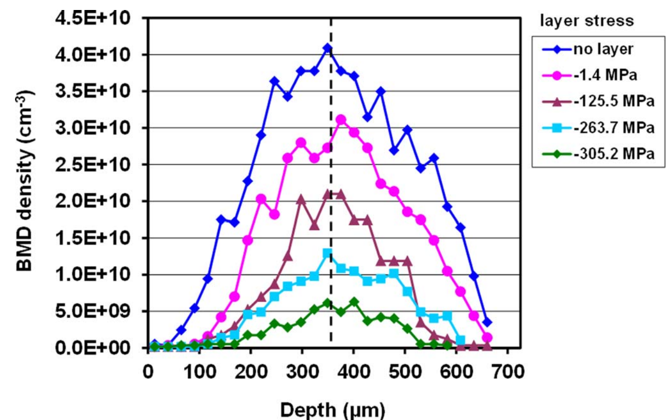

Figure 3. BMD density depth profiles in silicon covered by oxide layers with different layer stress after RTA at 1250°C for 30 s in Ar followed by 780°C 3 h and 1000°C 16 h both in N_2.

Downloaded on 2019-05-10 to IP 194.95.141.200 address. Redistribution subject to ECS terms of use (see ecsdl.org/site/terms_use) unless CC License in place (see abstract).

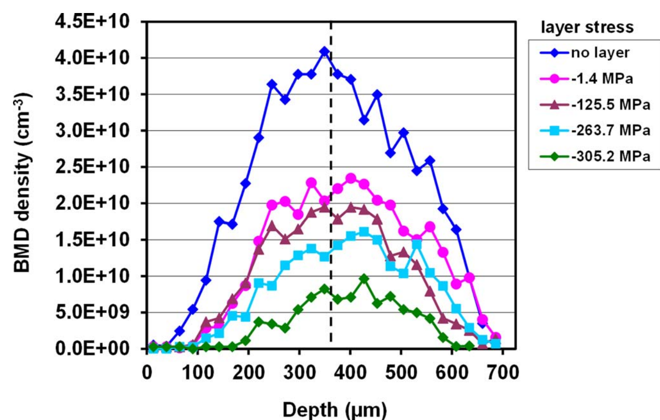

Figure 4. BMD density depth profiles in silicon covered by oxide layers with different layer stress after RTA at 1250°C for 30 s in Ar followed by 780°C 3 h and 1000°C 16 h both in N_2. The oxide layer was removed after the RTA.

increasing stress the BMD denuded zones below front and reverse surfaces increase and the BMD density in the bulk decreases.

Figure 4 shows the BMD depth profiles for RTA at 1250°C and BMD test but in this case the oxide layer was removed before the BMD test. Comparing the results with Fig. 3, it can be seen that there is not much difference. Only for the sample with layer stress −1.4 MPa the BMD density is somewhat lower if the oxide layer was removed prior to the BMD test.

The decrease of the average BMD density shown as a function of the layer stress is compared in Fig. 5 for the 1250°C RTA and BMD test with and without oxide layer. In both cases we can see that with increasing compressive stress the BMD density decreases. Even for a very low stress a clear decrease can be observed compared to a sample without layer. Both curves in Fig. 5 are very similar. This indicates that the RTA treatment is the most important step which defines the BMD density and profile.

For the RTA treatments at 1175°C no BMD depth profiles were generated because the BMD density for all samples was too low. Fig. 6 shows the average BMD densities for the 1175°C RTA and BMD test with and without oxide layer. A clear effect can be already observed if a nearly unstrained oxide layer exists on top of the wafer. For the 1175°C RTA, the BMD density is extremely low for all oxide layers. Thus, the oxide layers result in a very efficient suppression of oxygen precipitation if they are combined with a 1175°C RTA pre-treatment.

In Figs. 7 and 8, the results of the second set of experiments starting with nucleation anneals at 650°C followed by BMD tests are shown. As expected, the BMD density after 8 h of nucleation is higher than

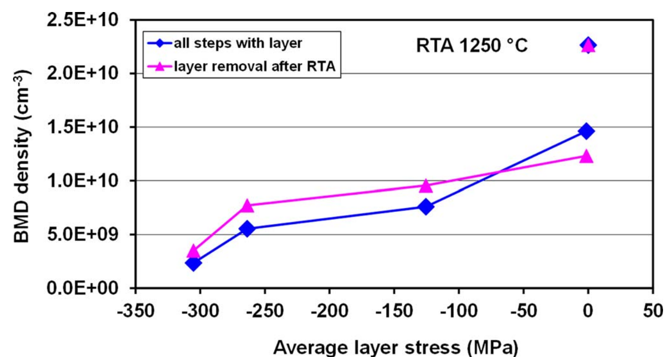

Figure 5. Average BMD density in silicon covered by oxide layers with different layer stress after RTA at 1250°C for 30 s in Ar followed by 780°C 3 h and 1000°C 16 h both in N_2. The results with and without removal of the oxide layer after the RTA are compared. The data points not connected by lines belong to samples without oxide layer.

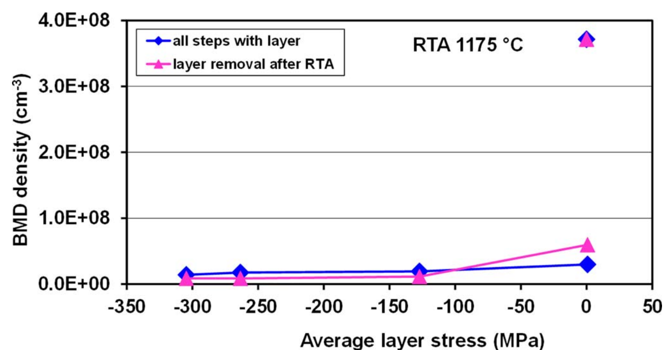

Figure 6. Average BMD density in silicon covered by oxide layers with different layer stress after RTA at 1175°C for 30 s in Ar followed by 780°C 3 h and 1000°C 16 h both in N_2. The results with and without removal of the oxide layer after the RTA are compared. The data points not connected by lines belong to samples without oxide layer.

after 4 h of nucleation. The BMD profiles are flat in all cases and of similar BMD density for each nucleation time. This indicates that neither the layer stress nor the existence of an oxide layer affects the nucleation of oxide precipitates.

Results of modeling.—The effect of RTA on the depth distribution of intrinsic point defects can be well explained considering both

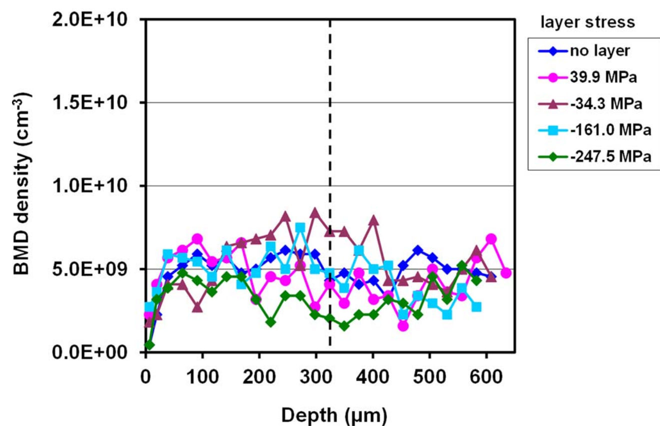

Figure 7. BMD density depth profiles in silicon covered by oxide layers with different layer stress after a nucleation anneal at 650°C for 4 h followed by 780°C 3 h and 1000°C 16 h all in N_2.

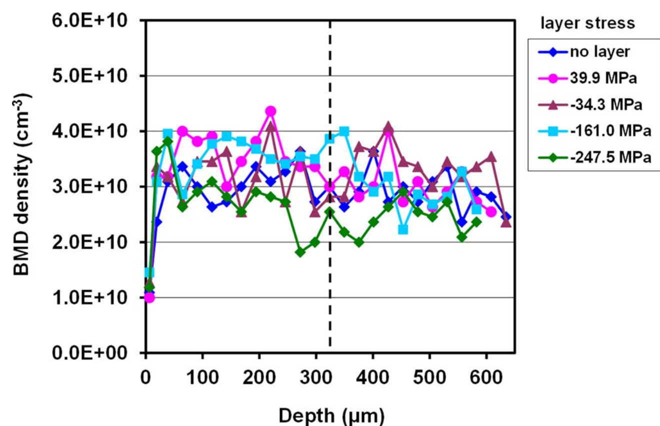

Figure 8. BMD density depth profiles in silicon covered by oxide layers with different layer stress after a nucleation anneal at 650°C for 8 h followed by 780°C 3 h and 1000°C 16 h, all in N_2.

Downloaded on 2019-05-10 to IP 194.95.141.200 address. Redistribution subject to ECS terms of use (see ecsdl.org/site/terms_use) unless CC License in place (see abstract).

diffusivity and solubility of the intrinsic point defects as a function of temperature.[22] In the region of temperature being important for our experiments, the diffusivity of interstitials is higher than the diffusivity of vacancies but the solubility of vacancies is higher than the solubility of interstitials.[23] For modeling, diffusion and the Frenkel pair formation[24] have to be taken into account, Then, the vacancy V and self-interstitial I depth profiles can be modeled using equations which describe the change of their concentrations as a function of time t and depth x:

$$\frac{\partial}{\partial t}C_{V,I}(x,t) = \frac{\partial}{\partial x}\left[D_{V,I}\frac{\partial}{\partial x}C_{V,I}(x,t)\right] - k_{IV}(x,t)[C_I(x,t)C_V(x,t) - C_I^{eq}(x,t)\,C_V^{eq}(x,t)]. \quad [2]$$

Here, $D_{V,I}$ are the diffusivities of interstitials and vacancies, $C_{V,I}$ are their concentrations, and $C_{V,I}^{eq}$ are their equilibrium concentrations. The Frenkel pair reaction constant k_{IV} can be obtained by

$$k_{IV}\,(x,t) = \frac{4\pi r_c}{\Omega C_{Si}}\,(D_I + D_V) \quad [3]$$

with the atomic density of silicon $C_{Si} = 5 \times 10^{22}\text{cm}^{-3}$, the capture radius $r_c = 10^{-7}$ cm, and the volume of the silicon unit cell $\Omega = 2.002 \times 10^{-23}\text{cm}^3$. The energy barrier of the Frenkel pair reaction was assumed to be zero.

The temperature profile T(t) recorded during the RTA treatment was used for the simulation. Start and end temperature was 400°C. The initial concentration of intrinsic point defects was set to their equilibrium values $C_{V,I}(x, 0\text{s}) = C_{V,I}^{eq}$. Dirichlet boundary conditions were used. At the reverse surface, $C_{V,I}\ (625\mu\text{m}, t) = C_{V,I}^{eq}\ (T)$ and at the front surface, $C_V\ (0\mu\text{m}, t) = C_V^{eq}\ (T)$ and $C_I\ (0\mu\text{m}, t) = S \cdot C_I^{eq}\ (T)$ were assumed, whereby the interstitial supersaturation S at the interface silicon/oxide is as follows

$$S = C_I(T)/C_I^{eq}(T). \quad [4]$$

The supersaturation was assumed to be constant. Because with this initial assumption very good adjustment to the experimental results was obtained, there was no need to use more complicated assumptions.

The result of this model are profiles of intrinsic point defects which need to be related to BMD profiles. In an earlier work, we found that the BMD density N is proportional to the third power of the vacancy supersaturation and to the sixth power of the supersaturation of interstitial oxygen.[25] Because it does not make sense to define equilibrium concentrations for a dynamic process like RTA, we simplify the relation to

$$N = a \cdot \left(C_V/10^{13}\right)^3 \cdot \left(C_{Oi}/10^{17}\right)^6 \quad [5]$$

and include the equilibrium concentrations into the constant fit factor a. Prerequisite for the obtained relationship is that the bulk BMD density is measured after 780°C 3 h and 1000°C 16 h. We used the same experimental values as in Ref. 26 for the BMD density in the bulk of wafers with oxygen concentrations in the range 4.8×10^{17} cm^{-3} to 7.8×10^{17} cm^{-3} and RTA treatments at temperatures in the range 1150°C to 1250°C for 10 s to 30 s in nitrogen and plotted them as function of the third power of the bulk vacancy concentration times the sixth power of the concentration of interstitial oxygen in Fig. 9 (left) and as function of the third power of the bulk vacancy concentration only in Fig. 9 (right). From the correlation in Fig. 9 (left) we obtain $a = 5.05 \times 10^3$ cm^{-24}. With the right graph in Fig. 9, we want to demonstrate that it is not sufficient to correlate the BMD density to a power of the vacancy concentration alone. This would work only in the case that all samples used are of the same initial concentration of interstitial oxygen as it was done in Ref. 27. Voronkov and Falster[28] also found a correlation of the BMD density with the third power of vacancies but they did not provide information about C_{Oi}.

In order to correlate the measured BMD density profiles with the results of modeling, we first determined a by adjusting a calculated profile with $S = 1$ to the measured profile of a wafer without oxide layer. In this case we found $a = 1.05 \times 10^5$ cm^{-24}. This value for a was used in all cases when the calculated vacancy concentration was converted into a BMD density using Eq. 5. In the next step, the modeled profiles of the BMD density were adjusted to the experimental BMD profiles of Figs. 3 and 4 using S as a fit factor. Figures 10 and 11 demonstrate that the experimental and modeled BMD depth profiles can be well adjusted. For RTA at 1175°C, it was not possible to measure BMD depth profiles because of the low BMD density. In this case we adjusted average BMD densities from experiment and simulation. The results can be found in Fig. 12. The BMD density of the sample without layer can be very well simulated using the value for a determined from RTA at 1250°C.

The resulting interstitial supersaturation at the silicon/oxide interface, shown in Fig. 13, is linearly increasing with increasing compressive layer stress. It is higher for RTA at 1175°C than for RTA at 1250°C. Even at zero stress, an interstitial supersaturation larger than one was found. The reason for this could be that during thermal treatment the layer stress changes by different thermal expansion of layer and substrate and by possible change of the internal stress by e.g. evaporation of hydrogen.

Discussion

We first want to discuss if hydrogen incorporated into the layers during PECVD enhances oxygen out-diffusion and in this way decreases oxygen precipitation. Newman found that hydrogen reduces

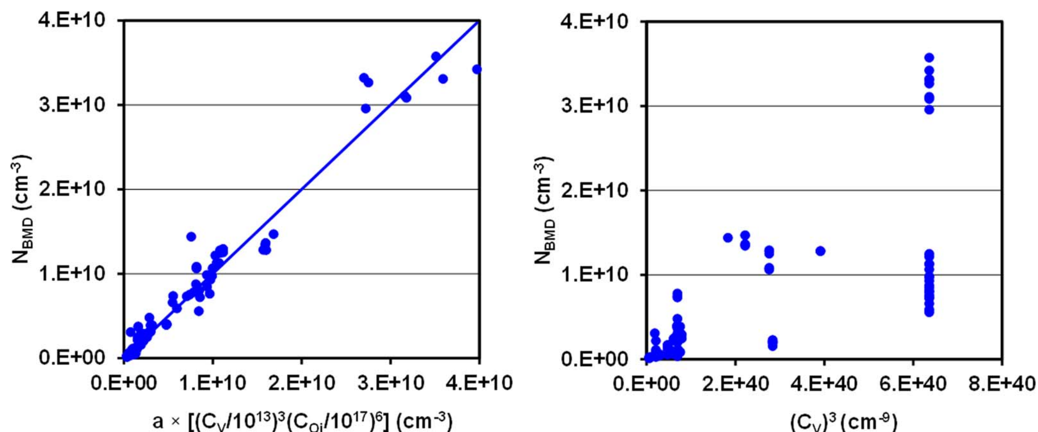

Figure 9. BMD density in the bulk of wafers with oxygen concentrations in the range 4.8×10^{17} cm^{-3} to 7.8×10^{17} cm^{-3} and RTA treatments at temperatures in the range 1150°C to 1250°C for 10 s to 30 s in nitrogen plotted as function of the third power of the bulk vacancy concentration times the sixth power of the concentration of interstitial oxygen (left) and as function of the third power of the bulk vacancy concentration only (right). BMD density was measured after 780°C 3 h and 1000°C 16 h in O_2.

Downloaded on 2019-05-10 to IP 194.95.141.200 address. Redistribution subject to ECS terms of use (see ecsdl.org/site/terms_use) unless CC License in place (see abstract).

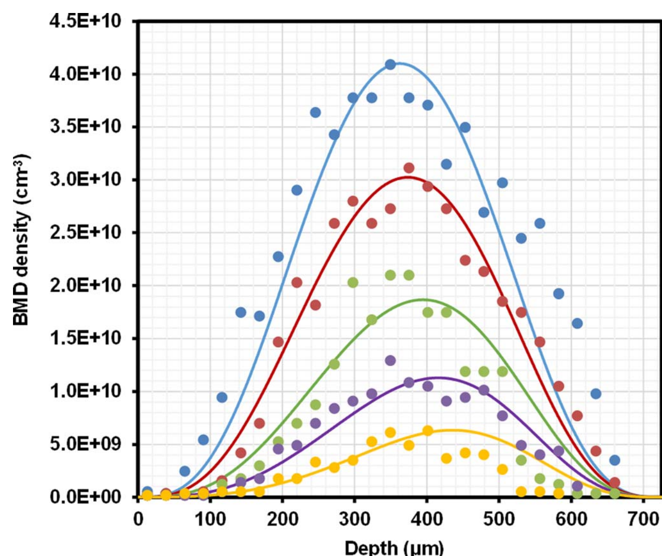

Figure 10. Comparison of modeled (lines) and measured (dots) BMD depth profiles in silicon covered by oxide layers with different layer stress after RTA at 1250°C for 30 s in Ar followed by 780°C 3 h and 1000°C 16 h both in N_2. Blue without layer, red −1.4 MPa, green −125.5 MPa, purple −263.7 MPa, and yellow −305.2 MPa layer stress.

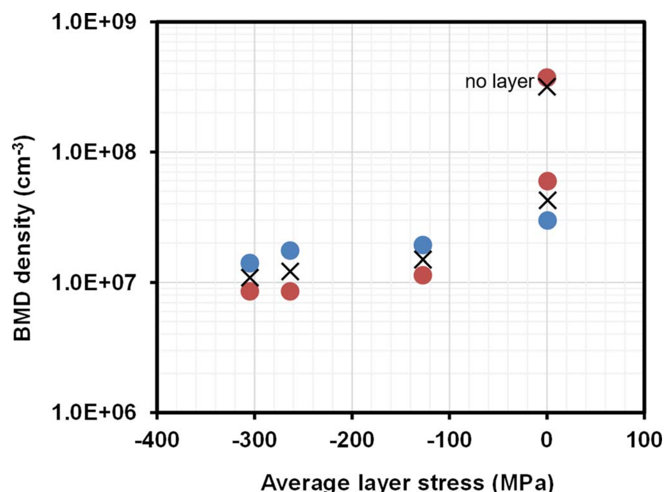

Figure 12. Comparison of modeled (black crosses) and measured (dots) average BMD densities in silicon covered by oxide layers with different layer stress after RTA at 1175°C for 30 s in Ar followed by 780°C 3 h and 1000°C 16 h both in N_2. On half of the samples the oxide layer was removed after the RTA (red dots) and on the other half it was left on (blue dots).

the migration barrier of oxygen and enhances the diffusivity of interstitial oxygen by the 10–1000 fold.[29] However, the hydrogen content of the layers decreases with increasing compressive layer stress but the BMD denuded zone increases. Even if hydrogen would diffuse into silicon during RTA at 1250°C, most of it would diffuse out again during the 3 h at 780°C before it can affect oxygen out-diffusion during the long anneal at 1000°C. For these reasons, we discarded hydrogen as a possible reason for the observed effects of strained oxide layers on the BMD depth profiles.

In most models for thermal oxidation, the self-interstitial supersaturation at the silicon/oxide interface is a function of the growth rate of the oxide layer.[1,5,6,27] With increasing temperature the self-interstitial supersaturation decreases.[27] We have chosen a deposition method for silicon oxide and not a thermal oxidation. Although a growth rate does not apply, we detected a self-interstitial supersaturation which increases with increasing compressive layer stress. Comparing our supersaturation values for RTA at 1250°C in Ar lying between 1.05 and 1.26 with the results of rapid thermal oxidation (RTO) published by Sudo et al.[27] for RTO at 1240°C lying between 1.1 and 1.23 it turns out that they are very similar. Also for the supersaturation determined for RTA at 1175°C the agreement with Ref. 27 is very good. Although there is good agreement with S from Sudo et al. at the RTA temperatures, it is not possible to model the measured BMD profiles with the assumption that the self-interstitial supersaturation further increases with decreasing temperature as described in Ref. 27. We also did not recognize an effect of self-interstitial supersaturation on nucleation of oxide precipitates at 650°C.

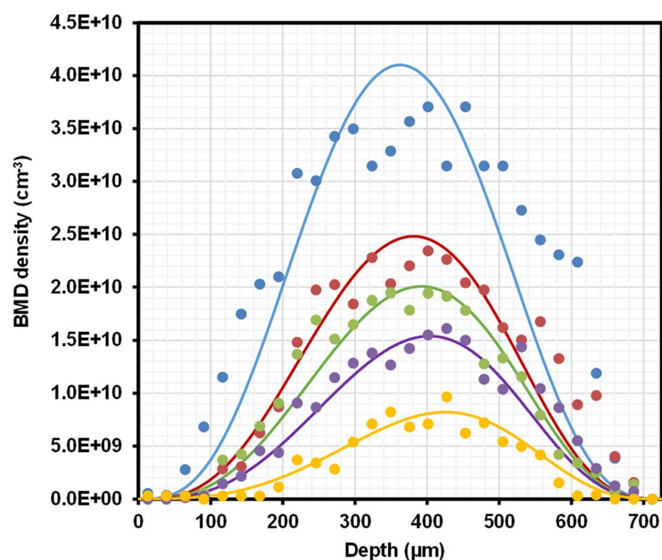

Figure 11. Comparison of modeled (lines) and measured (dots) BMD depth profiles in silicon covered by oxide layers with different layer stress after RTA at 1250°C for 30 s in Ar followed by 780°C 3 h and 1000°C 16 h both in N_2. The oxide layer was removed after the RTA. Blue without layer, red −1.4 MPa, green −125.5 MPa, purple −263.7 MPa, and yellow −305.2 MPa layer stress.

Conclusions

In order to investigate the effect of oxide layer stress on the generation of intrinsic point defects at the silicon/oxide interface, we have chosen a deposition method for silicon oxide and not a thermal oxidation. With PECVD it is possible to adjust the layer stress independent of the layer thickness. We deposited oxide layers of thicknesses in the

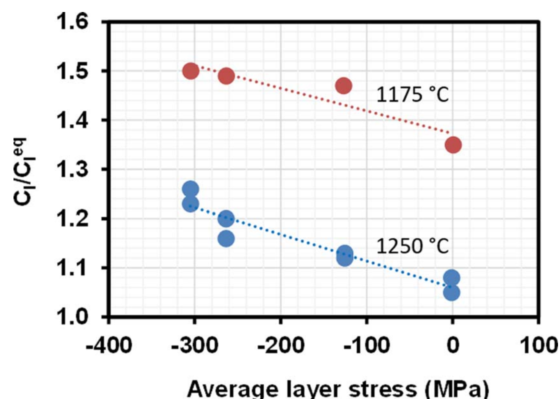

Figure 13. Supersaturation of self-interstitials as obtained from adjustment of modeling to experimental data plotted as function of the average layer stress for samples with RTA at 1250°C (blue dots) and with RTA at 1175°C (red dots).

Downloaded on 2019-05-10 to IP 194.95.141.200 address. Redistribution subject to ECS terms of use (see ecsdl.org/site/terms_use) unless CC License in place (see abstract).

range 799–869 nm with layer stresses ranging from −305.2 MPa to 39.9 MPa.

The intrinsic point defects generated were analyzed via their impact on oxygen precipitation. The BMD density is proportional to the product of the third power of the vacancy concentration and the sixth power of the concentration of interstitial oxygen if anneals at 780°C for 3 h + 1000°C for 16 h are used for stabilization and growth of oxide precipitates.

Supersaturations of self-interstitials as function of layer stress were determined by adjusting modelling results to measured BMD depth profiles. The self-interstitial supersaturation generated by RTA at 1250°C and 1175°C at the silicon/oxide interface is increasing linearly with increasing layer stress. Values for interstitial supersaturation determined on deposited oxide layers after RTA at 1250°C and 1175°C are very similar to values published for RTO by Sudo et al.[27]

An RTA 1175°C with a PECVD oxide on top of the wafer is a method to effectively suppress oxygen precipitation in silicon wafers. This is possible because the vacancy supersaturation generated by RTA at 1175°C is generally low and the additional in-diffusing interstitials further reduce its concentration.

Nucleation anneals carried out at 650°C for 4 h and 8 h did not show any effect of PECVD oxide layers on oxide precipitate nucleation.

ORCID

G. Kissinger https://orcid.org/0000-0002-6492-3117
D. Kot https://orcid.org/0000-0002-7857-5416

References

1. A. M. Agarwal and S. T. Dunham, *J. Appl. Phys.*, **78**, 5313 (1995).
2. P. M. Fahey, P. B. Griffin, and J. D. Plummer, *Rev. Mod. Phys.*, **61**, 289 (1989).
3. P. Fahey, G. Barbuscia, M. Moslehi, and R. W. Dutton, *Appl. Phys. Lett.*, **46**, 784 (1985).
4. S. T. Ahn, H. W. Kennel, J. D. Plummer, and W. A. Tiller, *Appl. Phys. Lett.*, **53**, 1593 (1988).
5. S. T. Dunham and N. Jeng, *Appl. Phys. Lett.*, **59**, 2016 (1991).
6. S. T. Dunham, *J. Appl. Phys.*, **71**, 685 (1992).
7. K. Taniguchi, Y. Shibata, and C. Hamaguchi, *J. Appl. Phys.*, **65**, 2723 (1989).
8. A. M.-R. Lin, R. W. Dutton, D. A. Antoniadis, and W. A. Tiller, *J. Electrochem. Soc.*, **128**, 1121 (1981).
9. J. Vanhellemont and C. Claeys, *J. Appl. Phys.*, **62**, 3960 (1987), *Erratum J. Appl. Phys.*, **71**, 1073 (1992).
10. C. Cui, D. Yang, X. Ma, R. Fan, and D. Que, *Phys. Stat. Sol. (a)*, **203**, 2370 (2006).
11. A. Antonelli and J. Bernholc, *Phys. Rev. B*, **40**, 10643 (1989).
12. K. Sueoka, E. Kamiyama, J. Vanhellemont, and K. Nakamura, *ECS Solid State Lett.*, **3**(6), P69 (2014).
13. K. Nakamura, R. Suewaka, and B. Ko, *ECS Solid State Letters*, **3**(3), N5 (2014).
14. M. J. Aziz, Y. Zhao, H.-J. Gossmann, S. Mitha, S. P. Smith, and D. Schiferl, *Phys. Rev. B*, **73**, 054101 (2006).
15. P. Pochet and D. Caliste, *Mat. Sci. in Semicond. Proc.*, **15**, 675 (2012).
16. M. Navi and S. T. Dunham, *J. Electrochem. Soc.*, **144**, 367 (1997).
17. G. G. Stoney, *Royal Society Proceedings*, **82**(A553), 172 (1909).
18. Secco d'Aragona, *J. Electrochem. Soc.*, **199**, 948 (1972).
19. A. C. Adams, F. B. Alexander, C. D. Capio, and T. E. Smith, *J. Electrochem. Soc.*, **128**, 1545 (1981).
20. J. C. Rostaing, Y. Cros, S. C. Gujrathi, and S. Poulain, *J. Non-Crystalline Solids*, **97&98**, 1051 (1987).
21. R. J. Jaccodine and W. A. Schlegel, *J. Appl. Phys.*, **37** (1966) 2429.
22. G. Kissinger, D. Kot, and W. von Ammon, *ECS J. Solid State Sci. Technol.*, **1**, P269 (2012).
23. T. A. Frewen and T. Sinno, *Appl. Phys. Lett.*, **89**, 191903 (2006).
24. J. Frenkel, *Kinetic theory of liquids*, Oxford Univ. Press, Oxford, 1946.
25. G. Kissinger and J. Dabrowski, *J. Electrochem. Soc.*, **155**, H448 (2008).
26. G. Kissinger, J. Dabrowski, A. Sattler, C. Seuring, T. Müller, H. Richter, and W. von Ammon, *J. Electrochem. Soc.*, **154**, H454 (2007).
27. H. Sudo, K. Nakamura, S. Maeda, H. Okamura, K. Izunome, and K. Sueoka, *ECS J. Solid State Science and Technology*, **8** (1), P35 (2019).
28. V. Voronkov and R. Falster, *Phys. Stat. Sol. B*, **251**, 2179 (2014).
29. R. Newman, *J. Phys.: Condensed Matter*, **12**, R335 (2000).

Downloaded on 2019-05-10 to IP 194.95.141.200 address. Redistribution subject to ECS terms of use (see ecsdl.org/site/terms_use) unless CC License in place (see abstract).